HHS Public Access

Author manuscript

Nat Commun. Author manuscript; available in PMC 2014 December 09.

Published in final edited form as:

Nat Commun. ; 5: 4075. doi:10.1038/ncomms5075.

Hypoxia-Inducible Hydrogels

Kyung Min Park and **Sharon Gerecht***

Department of Chemical and Biomolecular Engineering, Johns Hopkins Physical Sciences-Oncology Center, and the Institute for NanoBioTechnology, Johns Hopkins University, Baltimore, MD 21218

Abstract

Oxygen is vital for the existence of all multicellular organisms, acting as a signaling molecule regulating cellular activities. Specifically, hypoxia, which occurs when the partial pressure of oxygen falls below 5%, plays a pivotal role during development, regeneration, and cancer. Here we report a novel hypoxia-inducible (HI) hydrogel composed of gelatin and ferulic acid that can form hydrogel networks via oxygen consumption in a laccase-mediated reaction. Oxygen levels and gradients within the hydrogels can be accurately controlled and precisely predicted. We demonstrate that HI hydrogels guide vascular morphogenesis *in vitro* via hypoxia-inducible factors activation of matrix metalloproteinases and promote rapid neovascularization from the host tissue during subcutaneous wound healing. The HI hydrogel is a new class of biomaterials that may prove useful in many applications, ranging from fundamental studies of developmental, regenerative and disease processes through the engineering of healthy and diseased tissue models towards the treatment of hypoxia-regulated disorders.

Introduction

An emerging paradigm in the mimicry of three-dimensional (3D) microenvironments involves using a variety of bioinspired materials to reconstruct critical aspects of the native extracellular niche.[1, 2] Synthetic hydrogels have attracted substantial attention as 3D microenvironments owing to their structural similarity to the natural extracellular matrix (ECM) and their tunable properties.[3, 4] Researchers have endeavored to develop synthetic hydrogels to recapitulate temporal and spatial complexity in the native ECM, which varies not only in composition, but also in physicochemical parameters, including cell adhesion ligands,[5] growth factors/cytokines,[6] mechanical properties,[7] proteolytic degradability,[8] and topography.[9] Thus, these studies have established how such parameters individually or synergistically regulate cell behavior.

*Address for reprint request and other correspondence: S. Gerecht, Department of Chemical and Biomolecular Engineering, Johns Hopkins University Maryland Hall #116, Baltimore, MD 21218 Telephone: (410) 516-2846. gerecht@jhu.edu; Fax: (410) 516-5510.

Author contributions: K. M. Park designed and performed research, analyzed data, and wrote the paper; S. Gerecht designed research, analyzed data, and wrote the paper.

Competing financial interests statement: The authors declare no conflict of interest.

Oxygen (dioxygen, O_2) is vital for the existence of all multicellular organisms, acting as a signaling molecule for cells and regulating their metabolism, survival, cell-to-cell interactions, migration, and differentiation.[10, 11] Cellular responses to O_2 deprivation (hypoxia) are primarily regulated by hypoxia-inducible factors (HIFs) that accumulate under hypoxic conditions and activate the expression of numerous genes that regulate myriad cellular activities.[12] HIFs act as key regulators, promoting angiogenesis during embryonic development, tumor progression, and tissue regeneration.[13, 14, 15] HIFs regulate the expression of many angiogenic genes that promote vascular differentiation and morphogenesis, such as vascular endothelial growth factor (VEGF), VEGF receptor 2 (VEGFR2),[16, 17, 18] angiopoietin 1 (ANG1),[19] and matrix metalloproteinases (MMPs).[20, 21, 22, 23, 24] Although hypoxia plays a pivotal role in vascular development, nobody has simulated controlled hypoxia in a 3D microenvironment.

This study reports a new class of oxygen-controlling biomaterials, hypoxia-inducible (HI) hydrogels that can serve as 3D hypoxic microenvironments. We demonstrate control over and precise prediction of dissolved oxygen (DO) levels and gradients in the HI hydrogel. The HI hydrogel matrix stimulates tubulogenesis of endothelial-colony-forming cells (ECFCs) by activating HIFs and promotes rapid neovascularization from the host during subcutaneous wound healing. To our knowledge, this is the first hydrogel material with precisely controlled intramural DO levels - a new class of biomaterials for a wide range of possible applications.

Results

Design of HI hydrogels

We began by hypothesizing that conjugating ferulic acid (FA) to a polymer backbone would let us fabricate a HI hydrogel by consuming O_2 in laccase-mediated reactions. Though many fields (e.g., food chemistry and biosensors[25]) have explored such reactions, derived from phytochemistry, they have not yet been used to fabricate oxygen controllable biomaterials.

We selected gelatin (Gtn) as the polymer backbone for its cell-response properties, including cell adhesion sites and proteolytic degradability, which are critical in vascular morphogenesis.[26, 27] Gtn would enables a relatively simple functionalization with FA for the formation of intramural hypoxia for both *in vitro* and *in vivo* vascular inductions. This approach could also generate HI hydrogels using other natural/synthetic polymers, like polyethylene glycol, hyaluronic acid, and dextran. These might require incorporation of adhesion sites, such as Arg-Gly-Asp, and additional degradability features, such as MMP-sensitive peptides, depending on the application.[28, 29, 30]

We synthesized HI hydrogels by coupling carboxyl groups of FA to amine groups of Gtn (GtnFA) via a carbodiimide-mediated reaction (Supplementary Fig. 1; Supplementary Table 1.) and characterized the chemical structure of the functionalized polymer using ^{1}H NMR, indicating the specific peaks of anomeric carbon and alkyl protons of Gtn, as well as the aromatic protons of FA (Supplementary Fig. 2a). UV/VIS spectroscopy determined the degree of substitution (DS) of the FA molecule (Supplementary Fig. 2b). We fabricated the

HI hydrogel by crosslinking FA molecules *via* a laccase-mediated chemical reaction (Fig. 1a) to form diferulic acid (DiFA)[31], which yields polymer networks (Fig. 1b)[32].

To test hydrogel formation and viscoelastic modulus, we performed rheological analysis, including dynamic time sweep of hydrogels with varying laccase concentration (Fig. 2a-c). The crosslink point of elastic (G') and viscous (G'') modulus, which provides an estimate of the gelation time, occurs within 2 to 30 minutes, suggesting that laccase concentration affects the network formation kinetics. These data agree with the gelation kinetics observed by phase transition (Fig. 2d,e), suggesting that higher concentrations of laccase or polymer induce faster hydrogel formation. These results could have occurred because the rate of radical generation, which can induce DiFA formation, increased with higher laccase and polymer concentrations. Moreover, viscoelastic measurements showed tunable mechanical properties of the HI hydrogels (35 to 370 Pa), suggesting that they could maintain their 3D shapes, providing structural frameworks as extracellular microenvironments to support cell function. Another parameter to consider in designing cellular microenvironments, proteolytic degradability allows cell migration and niche remodeling.[4, 8] Thus, we examined protease-sensitive degradation of HI hydrogels. We observed that hydrogels incubated with collagenase degraded completely within three hours, the rate varying with the concentrations of collagenase (0.001 to 0.05%) and polymer (3 to 5%) solutions (Fig. 2e,g). These data demonstrate that the proteolytic degradability of the Gtn-based HI hydrogel is retained following functionalization with FA molecules.

We evaluated the cytocompatibility of hydrogels using human fibroblasts. We first examined the toxicity of the GtnFA conjugate and laccase, because precursor and free enzyme molecules have the potential to induce toxicity in a hydrogel matrix. We observed no significant cytotoxicity in the GtnFA polymer and laccase (80 to 98% of control) (Supplementary Fig. 3a,b). We also encapsulated fibroblasts within the HI hydrogels to determine cell viability and morphological changes within the matrix. The results show a predominantly viable fibroblast population, as well as cell spreading and elongation within HI hydrogel matrices (Supplementary Fig. 3c,d). Similar viability was observed when encapsulating ECFCs (Supplementary Fig. 3e). We demonstrate the successful preparation of cytocompatible HI hydrogels with tunable parameters essential for their use as a 3D cellular microenvironment [2, 4, 33].

Controllable oxygen levels and model predictions

We next hypothesized that GtnFA induces polymer network formation by O_2 consumption during hydrogel formation. To determine oxygen levels within the matrix, we monitored DO levels at the bottom of hydrogels using a noninvasive sensor patch.[34] We found that several factors — including hydrogel thickness, laccase concentrations, and DS values of polymer — affected DO levels and oxygen consumption rates.It should be noted that we used the same concentration of FA molecule, maintaining the same crosslinking density and thus diffusivity in all samples examined. Increasing laccase concentrations decreased both the DO levels and the time to reach the minimum DO level (DO_{min}), demonstrating that high laccase concentrations induce rapid O_2 consumption reactions and low O_2 levels (Fig. 3a). These data agree with the results of hydrogel formation studies, indicating that laccase

concentrations significantly affect both hydrogel network formation kinetics and oxygen consumption rates. Similarly, the higher DS value of FA molecules resulted in the lowest DO levels (Fig. 3b). Decreasing the FA content increased the DO_{min}. This is expected, since the FA molecule acts as a crosslinker, consuming O_2 molecules during hydrogel network formation.

Finally, we determined the influence of hydrogel thickness on DO levels. We varied gel thickness in a volume-dependent manner. Fig. 3c shows that controllable DO levels depend on the HI hydrogel thickness (3 wt%, DS 45, and 25 U/mL laccase). The DO_{min} decreased as thickness increased, demonstrating that intramural DO levels vary with matrix thickness. Notably, we observed DO levels within thick hydrogels (>2.5 mm) reaching hypoxic levels (<5%).

To enable accurate prediction of DO levels and gradients within HI hydrogels, we employed a mathematical model developed in our previous report.[34] We assumed that O_2 consumption kinetics during hydrogel formation follows Michaelis-Menten kinetics, as shown in equation (2). To accurately estimate DO gradients in HI hydrogels, we first determined the V_{max} and K_m parameters. We measured DO levels in hydrogels (3 wt%, DS45, and 25 U/mL laccase) until they reached steady state. We plotted the oxygen consumption rate of the laccase-mediated reaction (experimental data) and the theoretical Michaelis-Menten equation (numerical model) using the initial V_{max} and K_m values. We then calibrated the graphs while varying the V_{max} and K_m parameters to obtain the best fit to the experimental values according to the residual sum of squares (RSS) method (Supplementary Fig. 4). We determined that the V_{max} and K_m values of our HI hydrogels were 0.43 μM/second and 70 μM, respectively. We then compared the experimental DO values at the different hydrogel thicknesses to numerical DO values determined by the mathematical modeling to confirm the reliability of the given parameters. As can be seen, the experimental values are similar to the numerical model simulated by using the obtained V_{max} and K_m values (Fig. 3d). These results showed that the O_2 consumption rate (*e.g.*, hydrogel formation kinetics) follows the theoretical Michaelis-Menten equation.

Using the Michaelis-Menten parameters determined for the given conditions, we estimated the DO gradients throughout the gel depth in a two-layer (air-hydrogel) model. We found that,30 minutes after hydrogel formation, the DO levels at the bottom of hydrogels decreased as gel thickness increased, due to insufficient oxygen diffusion (Fig.3e), and a broad range of O_2 tensions occurred within the gel matrices (Fig. 3f). For instance, the O_2 gradient of the thin hydrogel (1.25 mm) ranged from 15 to 17%, while a thicker one (3.13 mm) exhibited a 1.8 to 21% range. Measurements of DO at different hydrogel depths confirmed the accuracy of the simulation, demonstrating DO gradient throughout the hydrogel matrix (Fig. 3g,h) and the robust effect of hydrogel thickness on O_2 levels and gradients.

Overall, oxygen measurements and computer simulations showed that our HI hydrogels consume O_2 during their formation, yielding an O_2 gradient within the matrix. Various factors could affect O_2 consumption rate and thus regulating not only the level of O_2 tensions but also the range of O_2 gradients. This is a very important advantage of the HI

hydrogels as oxygen gradients are generated in many tissues during embryonic development, tissue regeneration and cancer growth [13, 35, 36, 37, 38].Overall, the HI hydrogels may provide an innovative approach to generate hypoxic environments towards the delineation of the mechanism by which hypoxia regulates cellular responses and may facilitate the discovery of pathways involved in oxygen gradients environments.

Hypoxic microenvironment for vascular tube formation

We next speculated that HI hydrogel could provide controllable hypoxic environments to generate tissue models *in vitro*. Towards this, we selected an optimized hydrogel sample (3 wt% of polymer concentration, DS 45 of FA, and 25 U/mL of laccase) and controlled the DO levels by altering thickness.

We first performed computer simulation for media effects on O_2 gradients using a three-layer (air-media-hydrogel) model. As Fig. 3i,j shows, hydrogels placed in media for 30 minutes exhibited lower intramural DO levels. In fact, at thicknesses between 2.5 and 3.13 mm, DO levels were hypoxic (>5%) through the hydrogels' depth, suggesting their potential suitability for providing artificial hypoxic microenvironments. Towards using the HI hydrogel to study vascular morphogenesis, we chose to encapsulate ECFCs, which are capable of undergoing morphogenesis in synthetic matrices [26, 39]. We first determined how DO levels of hydrogels encapsulated with ECFCs depend on gel thickness. To test this, we encapsulated ECFCs within HI hydrogel matrices of different thickness (hypoxic gel, 2.50 mm; nonhypoxic gel [control], 1.25 mm), and cultured the constructs in ECFC media. Interestingly, the DO levels of the hypoxic gels decreased dramatically for the first 30 minutes and retained prolonged low O_2 levels for up to 50 hours (Fig. 3k), demonstrating that the HI hydrogel allowed the exposure of ECFCs to hypoxia and that the ECFCs also affected O_2 levels within the matrix. In fact, the DO levels of hypoxic gels without cells reached DO_{min} within 30 minutes, followed by a gradual increase after the inflection point, while the DO levels within the hypoxic gels encapsulating ECFCs remained hypoxic after DO_{min} for up to 50 hours (Fig. 3k) due to oxygen consumption by the cells. In contrast, nonhypoxic gels exhibited higher O_2 levels (>8%) than hypoxic gels but with a similar pattern, due to the encapsulated ECFCs.

We show that hypoxic environments can be generated and controlled in cultured HI hydrogels independently of cell encapsulation. Importantly, as O_2 consumption rates vary among different cell types, the HI hydrogel system provides opportunity to study hypoxia in diverse tissue models *in vitro*. We also show that the hypoxic environment in HI hydrogels is affected by the encapsulated ECFCs, which support continuous hypoxic environments.

To study the importance of the 3D hypoxic niche in cellular response, we next hypothesized that HI hydrogels would stimulate vascular morphogenesis through HIF pathway activation. To test this, we encapsulated ECFCs within HI hydrogel matrices of different thicknesses (hypoxic gel, 2.50 mm; nonhypoxic gel [control], 1.25 mm), and cultured them for up to three days. We observed different cell morphologies in hypoxic versus nonhypoxic gels. Unlike the limited sprout and tube formation of ECFCs within the nonhypoxic hydrogels, ECFCs within hypoxic gels underwent tubulogenesis, forming complex network structures after three days in culture (Fig. 4a). We also found significant increases in tube coverage,

length, and thickness (Fig. 4b-d), demonstrating that our HI hydrogels stimulate vascular morphogenesis. We observed more evolved vascular structures in hypoxic gels than in nonhypoxic gels, as demonstrated by 3D *z*–stack confocal analysis (Fig. 4e). We further noticed the formation of lumens in the vascular structures formed in hypoxic hydrogels, indicating mature vascular tube formation (Fig.4e and Supplementary Fig.5).

To better understand the molecular mechanisms underlying tube formation in HI hydrogels, we analyzed relevant gene expression soon after ECFC encapsulation. We found that ECFCs cultured in hypoxic gels expressed significantly higher levels of two isoforms of HIFα (HIF-1α and HIF-2α) after 12 hours than ECFCs within nonhypoxic hydrogels (Fig.5a). Interestingly, we found that HIF-1α gene expression gradually became upregulated in ECFCs in nonhypoxic gel for up to 24 hours during the culture period, probably due to the presence of FA molecules. A recent study demonstrated that free FA molecules could induce upregulation of HIF-1α expression in endothelial cells (ECs) in a concentration-dependent manner.[40] We also examined the expression of three MMP genes in ECFCs — membrane type 1 (MT1)-MMP, MMP-1, and MMP-2 — as these play a critical role in vascular morphogenesis.[26, 41, 42] We found that all MMP gene expressions in ECFCs from the hypoxic gel were upregulated over 48 hours of culture compared to ECFCs encapsulated in nonhypoxic gel (Fig.5b). We also confirmed protein levels and activities, finding higher levels of MT1-MMP and activated forms of MMP-1 and MMP-2 in hypoxic hydrogels (Supplementary Fig.6). Finally, we examined the gene expression of proangiogenic factors within the hypoxic microenvironment. We noticed upregulation of *VEGF* and *VEGFR2* in ECFCs encapsulated in hypoxic gels compared to nonhypoxic gels (Fig. 5c). *ANG1*, which contributes to blood vessel maturation and stabilization, was upregulated, while *ANG2*, an antagonist of *ANG1*, was downregulated in hypoxic hydrogels compared to nonhypoxic hydrogels. (Fig. 5c). Collectively, these results demonstrate that hypoxic hydrogels stimulate upregulation of proangiogenic and MMP genes affecting vascular morphogenesis.

To further understand the pathway activation that stimulates vascular morphogenesis within the HI hydrogels, we first performed a reoxygenation study. Reoxygenation, the phenomenon in which hypoxic regions become more exposed to oxygen by changing PO_2, induces production of reactive oxygen specimens, which involves an angiogenic response.[43] Our previous study demonstrated that reoxygenation affected the tube formation kinetics of ECs encapsulated in collagen gels in atmospheric conditions through a HIFα-independent pathway.[34] In our HI hydrogel system, we observed slight oxygen fluctuations (from 0.1 to 1.3% O_2) and a gradual increase after media changes (see Fig. 3k). Thus, we wondered if this slight reoxygenation due to media change affects vascular morphogenesis in the HI hydrogels. We encapsulated ECFCs within HI hydrogels and cultured them for up to three days with or without media changes. We found that ECFCs cultured without media changes underwent vascular morphogenesis similar to those cultured with media changes (Supplementary Fig. 7), demonstrating that reoxygenation does not affect the vascular morphogenesis of ECFCs in HI hydrogel systems. These results demonstrate that in contrast to existing hydrogel systems, which may provide uncontrolled and transient hypoxic environments, the HI hydrogel supports controllable and stable environments to activate hypoxia-regulated pathways.

We next aimed to determine whether vascular morphogenesis within HI hydrogels occurs through the activation of HIF. Small interfering RNA (siRNA) studies examined the involvement of HIF-1α and HIF-2α during ECFC tubulogenesis in HI hydrogels. We encapsulated ECFCs treated with either or both HIF siRNAs in HI hydrogels after confirming the suppression (Supplementary Fig. 8). Knocking down each or both HIFs reduced tube formation compared to untreated and luciferase-treated ECFCs (Fig. 5d) and Supplementary Fig. 9). Notably, when both HIFs were knocked down, most of the encapsulated ECFCs exhibited round shapes, even after three days in culture (Supplementary Fig. 9). To delineate whether vascular network formation in the HI hydrogel is regulated through HIF-secreted angiogenic growth factors, we examined the exogenous addition of Ang1 to the culture media (that already contains VEGF). We found that addition of Ang1 did not promote vascular network formation in the nonhypoxic hydrogels (Supplementary Fig. 10). Examining MT1-MMP, we detected significant downregulation of MT1-MMP expression after 24 hours of culture in the ECFCs treated with both HIFs siRNA compared to nontreated, luciferase-treated, and each HIF-treated-alone groups (Fig. 5e). When MT1-MMP was suppressed, encapsulated ECFCs did not generate vascular networks in HI hydrogels (Fig. 5f; Supplementary Fig. 11). Collectively, these results demonstrate that accumulation of HIF-1α and HIF-2α activates MT1-MMP, which enables vascular morphogenesis of ECFCs within HI hydrogels. Indeed, MT1-MMP was previously established as a critical component for the progression of 3D tubulogenesis within hydrogel materials.[26, 41, 42] In sum, our HI hydrogels, which can induce hypoxic microenvironments, promote complex and mature vascular tube structures by activating HIFs through the upregulated expression of proangiogenic factors and MMPs.

In vivo angiogenic effect of HI hydrogels

Although numerous studies have suggested that hypoxia stimulates blood vessel formation both *in vitro* and *in vivo*,[11, 23, 44] nobody has yet reported inducing acute hypoxia by manipulating a material-tissue interface to affect blood vessel invasion. To investigate the potential *in vivo* application of HI hydrogels, we hypothesized that our hypoxic hydrogel would induce acute hypoxia in surrounding tissues through *in situ* gel formation with oxygen consumption, which in turn would stimulate blood vessel invasion. We first performed a simulation to estimate DO levels after *in vivo* injection of hypoxic hydrogels using the given parameters. For this purpose, we assumed a partial pressure of oxygen in rat subcutaneous tissue of 40 mmHg, following previous reports,[45, 46] although the exact pressure was not defined. We found that the DO gradient from the center of the hydrogel to the hydrogel's edge (i.e the interface of the hydrogel and the surrounding tissue) is independent of the shape of the hydrogel (Fig. 6a-c). Notably, we found that DO levels at the edge of the hydrogel are lower than the physiological or pathological O_2 levels of the *in vivo* environments (from 10 mmHg to 40 mmHg; Fig. 6d-e), suggesting that HI hydrogels can induce an acutely hypoxic environment and may stimulate the surrounding tissues.

To confirm the effect of HI hydrogels on blood vessel recruitment *in vivo*, we generated two types of HI hydrogels (hypoxic and nonhypoxic). To control O_2 levels *in vivo*, we mixed calcium peroxide (CaO_2) as an oxygen-releasing compound to generate nonhypoxic gels (>8%O_2). To generate a hypoxic gel, we encapsulated calcium hydroxide — $Ca(OH)_2$ — a

side product of CaO_2 decomposition that does not influence the change of O_2 tension within the gel matrix (Supplementary Fig. 12). We injected the hydrogels subcutaneously to mice and examined them for up to five days. While microvasculature was observed surrounding both hydrogels, higher density and larger size of microvasculature were observed surrounding the hypoxic hydrogel than surrounding nonhypoxic gels after one day. After three and five days, the density of blood vessels surrounding and penetrating the hypoxic matrices increased to a greater extent than in nonhypoxic hydrogels (Fig.7a-d). Similar trends were observed in subcutaneous injections into rats (Supplementary Fig. 13). Evaluating whether the recruited blood vessels are anastomosed with the host vessels and are functional, we found that within three days, hypoxic hydrogels were invested with perfused microvasculature networks while isolated occasions of perfused microvasculature were detected in the nonhypoxic matrices (Fig. 8a) These perfused networks extended throughout the entire hypoxic hydrogels after five days while were limited in the nonhypoxic hydrogels (Fig. 8b**).**

Taken together, our results demonstrate that acute hypoxic conditions induced *in vivo* by the HI hydrogel promote blood vessel recruitment and neovascularization from the host during the wound-healing process. Thus, HI hydrogels can be further explored as an acellular matrix for the study of hypoxia-regulated cellular processes. In addition, HI hydrogels can be delivered through injection into the site of interest, thus requiring the use of minimally invasive techniques.

Discussion

The current study presents a new class of synthetic biomaterials that can mimic hypoxic conditions in native niches.Our novel approach demonstrated that HI hydrogels form via an enzyme-mediated reaction with oxygen consumption. We can accurately predict and control O_2 levels and gradients within our HI hydrogels, thus offering controllable and stable hypoxic environments. ECFCs encapsulated within HI hydrogel undergo morphogenesis and generate extensive vascular network structures via HIF-mediated activation of MT1-MMP. Hypoxic hydrogels promote blood vessel recruitment and infiltration via the material-tissue interface. To our knowledge, this is the first example of HI hydrogel materials. Moreover, this approach can be adapted for many other natural/synthetic polymers and may encourage innovation in a broad range of applications, including the study and treatment of hypoxia-regulated disorders, generation of artificial tissue constructs using progenitor or stem cells in regenerative medicine, and development of engineered *de novo* disease models such as *in vitro* cancer models.

Methods

Materials

Gelatin (Gtn, type A from porcine skin, less than 300 bloom), laccase (lyophilized powder from mushroom, ≥4.0 units/mg), 3-methoxy-4-hydroxycinnamic acid (ferulic acid, FA), *N*-(3-dimethylaminopropyl)-*N*′-ethylcarbodiimide hydrochloride (EDC), *N*-hydroxysuccinimide (NHS), dimethyl sulfoxide (DMSO), deuterium oxide (D_2O), and collagenase type IV were purchased from Sigma-Aldrich (Saint Louis, MO) and used as

obtained without purification. Dulbecco's Phosphate-Buffered Saline (DPBS), Dulbecco's Modified Eagle Medium (DMEM), and fetal bovine serum (FBS) were all purchased from Gibco, Invitrogen (Life Technologies, CA). Dialysis membrane (molecular cutoff = 3,500 Da) was purchased from Spectrum Laboratories (Rancho Dominguez, CA).

Synthesis of gelatin-*g*-ferulic acid

Gelatin-*g*-ferulic acid (GtnFA) conjugate was synthesized using EDC and NHS as coupling reagents. For the synthesis, a mixture of DMSO and distilled water (DIW) with a 1:1 volume ratio was prepared as a solvent. Gtn (1.0 g) was dissolved in 50 ml of the solvent at 40 °C. FA (0.78 g, 4.0 mmol) was dissolved in 20 ml of the solvent and reacted with EDC (0.92 g, 4.8 mmol, 1.2 eq. of carboxyl unit of FA) and NHS (0.64 g, 5.6 mmol, 1.4 eq. of carboxyl unit of FA) at room temperature for 15 minutes to activate the terminal carboxyl groups of FA. The activated solution was then applied to the Gtn solution and a conjugative reaction was conducted at 40 °C for 24 hours. After reaction, the solution was dialyzed against water for five days (MWCO = 3,500). After dialysis, we obtained GtnFA by freeze-drying and kept the product in a refrigerator before use. The degree of substitution (DS) of FA was measured using an UV/Vis spectrometer (SpectraMax; Molecular Devices, Sunnyvale, CA). GtnFA polymer (10 mg) was dissolved in 1 mL of a mixture of DMSO and DIW with a volume ratio of 1:1, and the absorbance was measured at the 320 nm wavelength. The concentration of the conjugated FA molecules was calculated from a calibration curve given by monitoring the absorbance of a known concentration of FA; it was standardized with the baseline measured using Gtn solution (10 mg/mL). The chemical structure of GtnFA was characterized using a ^{1}H NMR spectrometer (Bruker AMX-300 NMR spectrometer, Billerica, MA). The GtnFA polymer solution (10 mg/mL of D_2O) was prepared for the measurement. Supplementary Table 1 lists the synthesized polymer series depending on the feed amount of FA molecules.

Preparation of hypoxia-inducible hydrogels

Hypoxia-inducible (HI) hydrogels were prepared by mixing aqueous GtnFA polymer and laccase solution. Hydrogels (100 μl) were prepared in 1 ml vials at 37 °C. Seventeen five μL of the GtnFA polymer solution (4.0 to 6.7 wt%) and 25 μL of laccase solution (25 to 100 U/ml of stock solution) were simply mixed and gently shaken. To generate gel matrices of different thicknesses, we fabricated HI hydrogels in a 96-well plate (BD Bioscience or DO sensor patched plate-please see below for details) in a volume-dependent manner. For example, to generate hydrogel that was 2.5 mm thick, we pipetted 80 μL of the mixture of polymer and laccase solutions in each well and allowed them to react at 37 °C. All solutions used were dissolved in DPBS (pH 7.4), and the final concentration of the hydrogels was 3 to 5 wt%.

Gelation time

The gelation time of the HI hydrogels was determined by the vial-tilting method.[47] We prepared 100 μL of hydrogel in a 1 mL vial and mixed gently to initiate the crosslinking reaction at 37 °C. Gelation time was measured as the time point after inverting the solution

when more than three minutes passed without flow. The experiments were performed with different concentrations of laccase and polymer, as detailed in the article.

Measurement of viscoelastic properties

We performed rheological analysis of the HI hydrogels using a rheometric fluids spectrometer (RFS3, TA Instruments, New Castle, DE) with a 25 mm plate geometry.In the rheological experiments, hydrogel samples were prepared on the plate in the instrument. We performed dynamic time sweeps on hydrogel samples in various conditions. We monitored the elastic modulus (G') and viscous modulus (G'') at 10 percent of strain and a frequency of 0.1 Hz at 37 °C. A solvent trap wetted with deionized water was used to prevent sample evaporation.

In vitro proteolytic degradation study

In vitro degradation of HI hydrogels was gravimetrically determined. Hydrogels (100 μl) were prepared in microtubes and subsequently incubated in 500 μL of PBS with or without collagenease at 37 °C. We removed the media from the microtubes at a predetermined time and measured the weight of degraded hydrogels (W_d). Fresh media were added into the tube after weighing. The weight of the remaining hydrogels was then calculated according to the following equation (1):

$$Weight\ of\ hydrogel\ (\%) = (W_d / W_i) \times 100\,\% \quad (1)$$

where W_d is the weight of the degraded hydrogels and W_i is the weight of the initial hydrogels.

Cytocompatibility of HI hydrogels

All solutions for the *in vitro* cytotoxicity and viability studies were prepared using DPBS and filtered for sterilization using a syringe filter with a pore size of 0.2 μm. We investigated the cytotoxicity of the synthesized polymer and the enzyme using XTT (Sigma-Aldrich), according to the manufacturer's instructions and our previous report.[48] Briefly, newborn human foreskin fibroblasts (NUFF; Global Stem, Rockville, MD) were expanded. To test cytocompatability, 2.8×10^4 cells/cm^2 were cultured in 100 μL media and in the presence of polymer solution (0.63 to 10.0 mg/mL) or laccase solution (1.6 to 25 U/ml) for 24 hours, following by their incubation in medium containing 20 percent (v/v) XTT solution for four hours. For the quantitative analysis, we removed 100 μl of the medium, placed it in a 96-well plate, and read it in a microplate reader at the 450 nm wavelength. Cell viability was determined as a percentage of control cells (nontreated cells that were defined as 100% viable). Cell viability of HI hydrogels was evaluated using a live/dead kit (Invitrogen). Briefly, 5×10^5 NUFF cells/mL were encapsulated within HI hydrogels and cultured under standard cell culture conditions (37 °C and 5% CO_2) in high-glucose DMEM with 10% FBS. After incubation for 2 and 24 hours, we treated each well with 100 μl of 2 μM of the acetomethoxy derivate of calcein (calcein AM) and 4 μM of ethidium homodimer-1 (EthD-1) mixture and incubated at 37 °C for 30 minutes. The stained samples were washed three times using PBS and then counted with fluorescence microscopy (BX60, Olympus, Tokyo, Japan).

Dissolved oxygen measurement and mathematical model prediction

We measured DO levels noninvasively throughout hydrogels using commercially available sensor patches (Presens, Regensburg, Germany), as previously described.[34, 49, 50] To measure oxygen levels at the bottom of hydrogels, the polymer solutions were added on top of the sensors, which were immobilized in each well of a 96-well plate (BD Bioscience), and then mixed with laccase solutions. To measure oxygen levels within different regions of the hydrogel (top, 3 mm; middle, 1.5 mm), we measured oxygen levels using a simple device we designed (Supplementary Fig. 14). All experiments were conducted in a controlled environment at 37 °C and 5% CO_2 in incubators with and without culture media (DMEM plus 10% FBS). We controlled hydrogel thicknesses by varying the solution volume. DO gradients within the hydrogels were estimated using a mathematical model based on Michaelis-Menten kinetics, as described in our previous report.[34] Briefly, we assumed that the oxygen consumption rate (R) of laccase-mediated crosslinking reactions follow Michaelis-Menten kinetics (equation 2) and determined the Michaelis-Menten parameters of the oxygen-consuming hydrogel formation.

$$R=\frac{V_{\max}C_{O_2}}{K_m+C_{O_2}} \quad (2)$$

where V_{max} represents the maximum oxygen consumption rate and K_m is the oxygen concentration at which the reaction rate is half of V_{max}. To determine these parameters, we measured the steady-state DO level of 3 wt% hydrogel (DS 45) formed with 25.0 U/mL laccase and plotted the experimental data using the Michaelis-Menten equation. We also calibrated the plots according to the residual sum of squares (RSS) method to give the best-fit graphs between the theoretical equation and experimental values. We simulated the two-layer (air-hydrogel) and three-layer (air-media-hydrogel) models of the DO gradients with commercial software, Comsol Multiphysics (Comsol, LA, CA), as previously described.[51]

ECFC encapsulation and viability

All solutions for the *in vitro* viability were prepared using DPBS and filtered for sterilization using a syringe filter with a pore size of 0.2 μm. ECFCs (Lonza, Walkersville, MD) were cultured, as previously described,[52] in endothelial growth media-2 (EGM2; Lonza) containing VEGF and 10% FBS on the plate coated with type I collagen (BD Biosciences, Franklin Lakes, NJ). GtnFA polymer solution (4 wt%) was dissolved in PBS (pH 7.4) and mixed with ECFC pellets to provide cell suspension, and then laccase solution (100 U/mL) was added at a volume ratio of 3:1 (polymer solution:laccase solution) and gently mixed for two minutes 37 °C. The final concentration of the polymer, laccase, and cells were 3 wt%, 25 U/mL, and 2×10^6 cells/mL, respectively. The mixture was placed in the 96-well plate and allowed to react at 37 °C for 15 minutes. The ECFCs encapsulated within the hydrogels were cultured with 200 μL in growth media (Lonza) under standard cell culture conditions (37 °C and 5% CO_2) for up to 72 hours. The culture medium was replaced every 24 hours. For viability, after incubation for 24 and 72 hours, we treated each well with 100 μl of 2 μM of calcein AM and 1 μM of EthD-1 mixture, incubate and analyzed as detailed above for NUFF cells. We observed the ECFCs at different region of hydrogels by controlling the

coaxial coarse/fine-focusing knob of microscope. ECFC morphologies were observed using optical microscopy (in phase-contrast mode) and confocal microscopy (LSM 510 Meta, Carl Zeiss). For confocal observations, ECFCs within hydrogels were fixed using 3.7% paraformaldehyde for 40 minutes at room temperature and washed three times using PBS. The fixed cells were permeabilized with 0.1% Triton X-100 for 20 minutes and incubated with 1% BSA blocking solution at room temperature for one hour. The hydrogel samples were incubated with phalloidin (1:40; Molecular Probes, Eugene, OR) and Hoechst 33258 (1:10,000; Molecular Probes) to visualize the cytoplasm and nuclei, respectively.

Real-time RT-PCR

Quantitative real time RT-PCR was performed as described previously.[26, 52] Briefly, total RNA was isolated from ECFCs encapsulated in hydrogels using TRIzol (Invitrogen) according to the manufacturer's instructions. Total RNA was quantified using an ultraviolet spectrophotometer and validated for having no DNA contamination. RNA (1 μg/sample) was transcribed using reverse transcriptase M-MLV and oligo(dT) primers (both from Promega Co., Madison, WI) according to the manufacturer's instructions. We used TaqMan Universal PCR MasterMix and Gene Expression Assay (Applied Biosystems, Foster City, CA) according to the manufacturer's instructions for *HIF-1α, HIF-2α, VEGF, VEGFR, ANG1, ANG2, MT1-MMP, MMP-1, MMP-2*- and *β-actin*, as described previously.

Live staining and angiogenesis assay

We performed live staining using Calcein-AM (Invitrogen) to quantify the mean tube coverage, length, and thickness, as described previously.[34] Briefly, ECFCs were encapsulated and cultured for three days using the above-described method. One hundred microliter of 2 μM calcein solution was added to each well, and the ECFCs embedded in the hydrogel were incubated at room temperature for 60 minutes. The stained cells were washed three times using PBS and then observed with fluorescence microscopy (BX60, Olympus, Tokyo, Japan). For the angiogenesis analysis, we use 5-20 images at 20× magnifications of different fields within the hydrogels, and the vascular tube structure was analyzed using MetaMorph software (Universal Imaging, Downingtown, PA) with the angiogenesis tools.

Effect of ANG-1 on ECFC vascular morphogenesis in HI hydrogels

We encapsulated ECFCs within HI hydrogels (hypoxic *vs.*nonhypoxic gel) as described above, and cultured them in EGM2 (Lonza) containing 10% FBS with additional 50 ng/mL of ANG-1. ECFC morphologies were observed using optical microscopy (in phase-contrast mode) along the three-day culture period.

Zymography

We collected the conditioned media from each condition at predetermined time points and analyzed for MMP-1 and MMP-2 as previously described.[39] In brief, collected media were loaded on 10% gelatin (for MMP-2) and 12% casein (for MMP-1) zymography gels (Bio-Rad, Hercules, CA). We performed electrophoresis for 90 minutes at room temperature. After washing the gels in water, SDS was extracted from the gels with renaturation buffer

(Invitrogen). MMP activities were developed in a developing buffer (Invitrogen) at 37 °C for 24 hours and visualized by staining with Coomassie Blue R-250.

Western blot

We performed western blot analysis as described previously.[52] Cell lysates were prepared in a Tris-Triton-X buffer (1% Trion-X, 150 mM NaCl, and 50 mM Tris, pH 7.5) with 1 × protease inhibitor cocktail (Thermo Scientific, Waltham, Ma). Protein isolated from cell lysates was quantified with the DC assay (Bio-Rad) and boiled at 95 °C for five minutes in Laemmli buffer (Bio-Rad) with β-mercaptoethanol. Protein (25 μg/well) was loaded into a 4 to 20 percent SDS-PAGE gel (Bio-Rad). Proteins were transferred to nitrocellulose membranes, blocked in three percent nonfat milk for one hour, and incubated overnight at 4 °C (under constant shaking) with primary antibody: rabbit anti-MMP14 (MT1-MMP, 1:1,000) and GAPDH (1:3,000; both from Abcam, Cambridge, MA). We washed the membranes three times in Tris-buffered saline containing 0.1% Tween 20 (TBST) for 15 minutes each and incubated with anti-rabbit horseradish peroxidase (HRP) (1:1,000; Cell Signaling Technology, Danvers, MA). Membranes were washed three times in TBST, developed with enhanced chemiluminescence (Pierce), and visualized using the ChemiDoc XRS+ System (Bio-Rad).

Small interfering RNA transfection

ECFCs were transfected with siGENOME SMARTpool human HIF-1α, HIF-2α and MT1-MMP (Dharmacon, Lafayette, CO) following the manufacture's protocol, as previously described.[26, 51, 52] Cells were seeded on a six-well plate and treated with 100 nM siRNA. We performed mRNA analysis after 24 hours and used confirmed transfected cells for experiments after 48 hours.

In vivo subcutaneous injection

We performed subcutaneous injection in rats (n=6, 6-10 week-old Sprague dawley female) or mice (n=4, 6-10 week-old C57/6 female) to investigate the *in vivo* angiogenic effects of HI hydrogels. To control oxygen levels *in vivo*, we mixed a small amount of calcium peroxide (CaO_2; Sigma-Aldrich) and calcium hydroxide — $Ca(OH)_2$ (Sigma-Aldrich) — with the polymer solution. The solid calcium peroxide begins to decompose and release O_2 molecules when in contact with water.[53] Thus, we encapsulated CaO_2 as an oxygen-releasing compound to generate nonhypoxic hydrogel as a control group. In order to minimize the difference between the sample groups, we also encapsulated $Ca(OH)_2$, a by-product of CaO_2 decomposition, within hypoxic hydrogels. $Ca(OH)_2$ does not influence the change of O_2 tension within the gel matrix. In our initial study, we optimized concentrations of calcium derivatives to control oxygen levels for *in vivo* studies. We injected two hundred microliters of hydrogels formed with 0.02% $Ca(OH)_2$ (hypoxic hydrogel) and the same volume of hydrogels formed with 0.02% CaO_2 (nonhypoxic hydrogel) into the backs of rats (four to six weeks old). For this study, polymer solutions were sterilized by filtering using syringe filter (pore size, 0.2 μm) and injected using 26-gauge needles. At each predetermined time point (one, three and five days), we sacrificed the animals, removed the hydrogels with the surrounding tissue, fixed the explants in formalin-free Accustain fixative,

and proceeded to histological analysis. To confirm the vascular functionality of blood vessels infiltrated into hydrogel matrix, we injected Alexa Fluor 568-conjugated isolectin GS-IB4 from *Griffonia simplicifolia* (Invitrogen) through the tail veins of the mice, as we previously described.[54] After 30 min, we sacrificed the mice, removed the hydrogels, stained with Hoechst, and then proceeded for visualization using confocal microscopy (LSM 510 Meta, Carl Zeiss). The animal study was performed using a protocol (RA11A196 and MO12A210) approved by The Johns Hopkins University Institutional Animal Care and Use Committee.

Histological analysis

After we fixed the explants as described above, the samples were then dehydrated in graded ethanol (80 to 100%), embedded in paraffin, serially sectioned using a microtome (5 μm), and stained with either hematoxylin and eosin (H&E) or underwent immunohistochemistry for α-SMA and CD31 as previously.

Statistical analysis

We performed all measurements of hydrogel characterizations, including gelation time, proteolytic degradation, and mechanical strength, using triplicate samples for each data point. We performed RT-PCR analysis for HIFs, MMPs, and proangiogenic factors in triplicate with duplicate readings. We performed statistical analysis using GraphPad Prism 4.02 (GraphPad Software Inc., La Jolla, CA). We also used this software to perform *t*–tests to determine significance. Significant levels, determined using post-tests, were set at: $*p < 0.05$, $**p < 0.01$, and $***p < 0.001$. All graphical data were reported.

Supplementary Material

Refer to Web version on PubMed Central for supplementary material.

Acknowledgments

We thank S. Kusuma for critically reviewing this paper; A. Hielscher for assistance with zymography and western blot; H. E. Abaci for technical assistance with oxygen measurement, RT-PCR, and reoxygenation studies; Y. I. Shen for assistance with *in vivo* animal injection and immunohistochemistry; S. F. Barreto for assistance with ECFCs culture. This work was supported by NIH grants R01HL107938 and U54CA143868 and National Science Foundation grant 1054415 (to S.G).

References

1. Huebsch N, Mooney DJ. Inspiration and application in the evolution of biomaterials. Nature. 2009; 462:426–432. [PubMed: 19940912]
2. Place ES, Evans ND, Stevens MM. Complexity in biomaterials for tissue engineering. Nat Mater. 2009; 8:457–470. [PubMed: 19458646]
3. Cushing MC, Anseth KS. Hydrogel cell cultures. Science. 2007; 316:1133–1134. [PubMed: 17525324]
4. Lutolf MP, Hubbell JA. Synthetic biomaterials as instructive extracellular microenvironments for morphogenesis in tissue engineering. Nat Biotechnol. 2005; 23:47–55. [PubMed: 15637621]
5. Luo Y, Shoichet MS. A photolabile hydrogel for guided three-dimensional cell growth and migration. Nat Mater. 2004; 3:249–253. [PubMed: 15034559]

6. Martino MM, et al. Engineering the growth factor microenvironment with fibronectin domains to promote wound and bone tissue healing. Sci Transl Med. 2011; 3:100ral189.
7. Engler AJ, Sen S, Sweeney HL, Discher DE. Matrix elasticity directs stem cell lineage specification. Cell. 2006; 126:677–689. [PubMed: 16923388]
8. Lutolf MP, et al. Synthetic matrix metalloproteinase-sensitive hydrogels for the conduction of tissue regeneration: engineering cell-invasion characteristics. Proc Natl Acad Sci U S A. 2003; 100:5413–5418. [PubMed: 12686696]
9. Kilian KA, Bugarija B, Lahn BT, Mrksich M. Geometric cues for directing the differentiation of mesenchymal stem cells. Proc Natl Acad Sci U S A. 2010; 107:4872–4877. [PubMed: 20194780]
10. Semenza GL. Life with oxygen. Science. 2007; 318:62–64. [PubMed: 17916722]
11. Covello KL, Simon MC. HIFs, hypoxia, and vascular development. Curr Top Dev Biol. 2004; 62:37–54. [PubMed: 15522738]
12. Keith B, Simon MC. Hypoxia-inducible factors, stem cells, and cancer. Cell. 2007; 129:465–472. [PubMed: 17482542]
13. Simon MC, Keith B. The role of oxygen availability in embryonic development and stem cell function. Nat Rev Mol Cell Biol. 2008; 9:285–296. [PubMed: 18285802]
14. Heddleston JM, Li Z, Lathia JD, Bao S, Hjelmeland AB, Rich JN. Hypoxia inducible factors in cancer stem cells. Br J Cancer. 2010; 102:789–795. [PubMed: 20104230]
15. Jopling C, Sune G, Faucherre A, Fabregat C, Izpisua Belmonte JC. Hypoxia induces myocardial regeneration in zebrafish. Circulation. 2012; 126:3017–3027. [PubMed: 23151342]
16. Ferrara N, Gerber HP, LeCouter J. The biology of VEGF and its receptors. Nat Med. 2003; 9:669–676. [PubMed: 12778165]
17. Lee YM, et al. Determination of hypoxic region by hypoxia marker in developing mouse embryos in vivo: a possible signal for vessel development. Dev Dyn. 2001; 220:175–186. [PubMed: 11169851]
18. Gassmann M, et al. Oxygen supply and oxygen-dependent gene expression in differentiating embryonic stem cells. Proc Natl Acad Sci U S A. 1996; 93:2867–2872. [PubMed: 8610133]
19. Augustin HG, Koh GY, Thurston G, Alitalo K. Control of vascular morphogenesis and homeostasis through the angiopoietin-Tie system. Nat Rev Mol Cell Biol. 2009; 10:165–177. [PubMed: 19234476]
20. Fong GH. Regulation of angiogenesis by oxygen sensing mechanisms. J Mol Med. 2009; 87:549–560. [PubMed: 19288062]
21. Manalo DJ, et al. Transcriptional regulation of vascular endothelial cell responses to hypoxia by HIF-1. Blood. 2005; 105:659–669. [PubMed: 15374877]
22. Ottino P, et al. Hypoxia activates matrix metalloproteinase expression and the VEGF system in monkey choroid-retinal endothelial cells: Involvement of cytosolic phospholipase A2 activity. Mol Vision. 2004; 10:341–350.
23. Pugh CW, Ratcliffe PJ. Regulation of angiogenesis by hypoxia: role of the HIF system. Nat Med. 2003; 9:677–684. [PubMed: 12778166]
24. Ben-Yosef Y, Lahat N, Shapiro S, Bitterman H, Miller A. Regulation of endothelial matrix metalloproteinase-2 by hypoxia/reoxygenation. Circ Res. 2002; 90:784–791. [PubMed: 11964371]
25. Rosana CM, Glasucia MP, Nelson D. Potential applications of laccase in the food industry. Trends Food Sci Technol. 2002; 13:205–216.
26. Hanjaya-Putra D, et al. Controlled activation of morphogenesis to generate a functional human microvasculature in a synthetic matrix. Blood. 2011; 118:804–815. [PubMed: 21527523]
27. Davis GE, Senger DR. Endothelial extracellular matrix: biosynthesis, remodeling, and functions during vascular morphogenesis and neovessel stabilization. Circ Res. 2005; 97:1093–1107. [PubMed: 16306453]
28. Cuchiara MP, Gould DJ, McHale MK, Dickinson ME, West JL. Integration of Self-Assembled Microvascular Networks with Microfabricated PEG-Based Hydrogels. Adv Funct Mater. 2012; 22:4511–4518. [PubMed: 23536744]

29. Khetan S, Guvendiren M, Legant WR, Cohen DM, Chen CS, Burdick JA. Degradation-mediated cellular traction directs stem cell fate in covalently crosslinked three-dimensional hydrogels. Nat Mater. 2013; 12:458–465. [PubMed: 23524375]
30. DeForest CA, Polizzotti BD, Anseth KS. Sequential click reactions for synthesizing and patterning three-dimensional cell microenvironments. Nat Mater. 2009; 8:659–664. [PubMed: 19543279]
31. Grabber JH, Hatfield RD, Ralph J, Zon J, Amrhein N. Ferulate Cross-Linking in Cell-Walls Isolated from Maize Cell-Suspensions. Phytochemistry. 1995; 40:1077–1082.
32. Riva S. Laccases: blue enzymes for green chemistry. Trends Biotechnol. 2006; 24:219–226. [PubMed: 16574262]
33. Tibbitt MW, Anseth KS. Hydrogels as extracellular matrix mimics for 3D cell culture. Biotechnol Bioeng. 2009; 103:655–663. [PubMed: 19472329]
34. Abaci HE, Truitt R, Tan S, Gerecht S. Unforeseen decreases in dissolved oxygen levels affect tube formation kinetics in collagen gels. Am J Physiol Cell Physiol. 2011; 301:C431–440. [PubMed: 21543738]
35. Griffith LG, Swartz MA. Capturing complex 3D tissue physiology in vitro. Nat Rev Mol Cell Biol. 2006; 7:211–224. [PubMed: 16496023]
36. Helmlinger G, Yuan F, Dellian M, Jain RK. Interstitial pH and pO2 gradients in solid tumors in vivo: high-resolution measurements reveal a lack of correlation. Nat Med. 1997; 3:177–182. [PubMed: 9018236]
37. Hunt TK, Zederfeldt B, Goldstick TK. Oxygen and healing. Am J Surg. 1969; 118:521–525. [PubMed: 4898193]
38. Remensnyder JP, Majno G. Oxygen gradients in healing wounds. Am J Pathol. 1968; 52:301–323. [PubMed: 5635856]
39. Hanjaya-Putra D, Wong KT, Hirotsu K, Khetan S, Burdick JA, Gerecht S. Spatial control of cellmediated degradation to regulate vasculogenesis and angiogenesis in hyaluronan hydrogels. Biomaterials. 2012; 33:6123–6131. [PubMed: 22672833]
40. Lin CM, Chiu JH, Wu IH, Wang BW, Pan CM, Chen YH. Ferulic acid augments angiogenesis via VEGF, PDGF and HIF-1 alpha. J Nutr Biochem. 2010; 21:627–633. [PubMed: 19443196]
41. Chun TH, et al. MT1-MMP-dependent neovessel formation within the confines of the three-dimensional extracellular matrix. J Cell Biol. 2004; 167:757–767. [PubMed: 15545316]
42. Stratman AN, et al. Endothelial cell lumen and vascular guidance tunnel formation requires MT1-MMP-dependent proteolysis in 3-dimensional collagen matrices. Blood. 2009; 114:237–247. [PubMed: 19339693]
43. Pan Y, et al. Multiple factors affecting cellular redox status and energy metabolism modulate hypoxia-inducible factor prolyl hydroxylase activity in vivo and in vitro. Mol Cell Biol. 2007; 27:912–925. [PubMed: 17101781]
44. Marti HJ, et al. Hypoxia-induced vascular endothelial growth factor expression precedes neovascularization after cerebral ischemia. Am J Pathol. 2000; 156:965–976. [PubMed: 10702412]
45. Fischer B, Bavister BD. Oxygen tension in the oviduct and uterus of rhesus monkeys, hamsters and rabbits. J Reprod Fertil. 1993; 99:673–679. [PubMed: 8107053]
46. Zhang Y, Wilson GS. In vitro and in vivo evaluation of oxygen effects on a glucose oxidase based implantable glucose sensor. Anal Chim Acta. 1993; 281:513–520.
47. Park KM, Ko KS, Joung YK, Shin H, Park KD. In situ cross-linkable gelatin-poly(ethylene glycol)-tyramine hydrogel via enzyme-mediated reaction for tissue regenerative medicine. J Mater Chem. 2011; 21:13180–13187.
48. Sun G, Shen YI, Ho CC, Kusuma S, Gerecht S. Functional groups affect physical and biological properties of dextran-based hydrogels. J Biomed Mater Res Part A. 2010; 93:1080–1090.
49. Abaci HE, Truitt R, Luong E, Drazer G, Gerecht S. Adaptation to oxygen deprivation in cultures of human pluripotent stem cells, endothelial progenitor cells, and umbilical vein endothelial cells. Am J Physiol Cell Physiol. 298:C1527–1537. [PubMed: 20181925]
50. Abaci HE, Devendra R, Smith Q, Gerecht S, Drazer G. Design and development of microbioreactors for long-term cell culture in controlled oxygen microenvironments. Biomed Microdevices. 2012; 14:145–152. [PubMed: 21947550]

51. Abaci HE, Truitt R, Tan S, Gerecht S. Unforeseen decreases in dissolved oxygen levels affect tube formation kinetics in collagen gels. Am J Physiol Cell Physiol. 301:C431–440. [PubMed: 21543738]

52. Kusuma S, Zhao S, Gerecht S. The extracellular matrix is a novel attribute of endothelial progenitors and of hypoxic mature endothelial cells. FASEB J. 2012; 26:4925–4936. [PubMed: 22919069]

53. Oh SH, Ward CL, Atala A, Yoo JJ, Harrison BS. Oxygen generating scaffolds for enhancing engineered tissue survival. Biomaterials. 2009; 30:757–762. [PubMed: 19019425]

54. Kusuma S, Shen YI, Hanjaya-Putra D, Mali P, Cheng L, Gerecht S. Self-organized vascular networks from human pluripotent stem cells in a synthetic matrix. Proc Natl Acad Sci U S A. 2013; 110:12601–12606. [PubMed: 23858432]

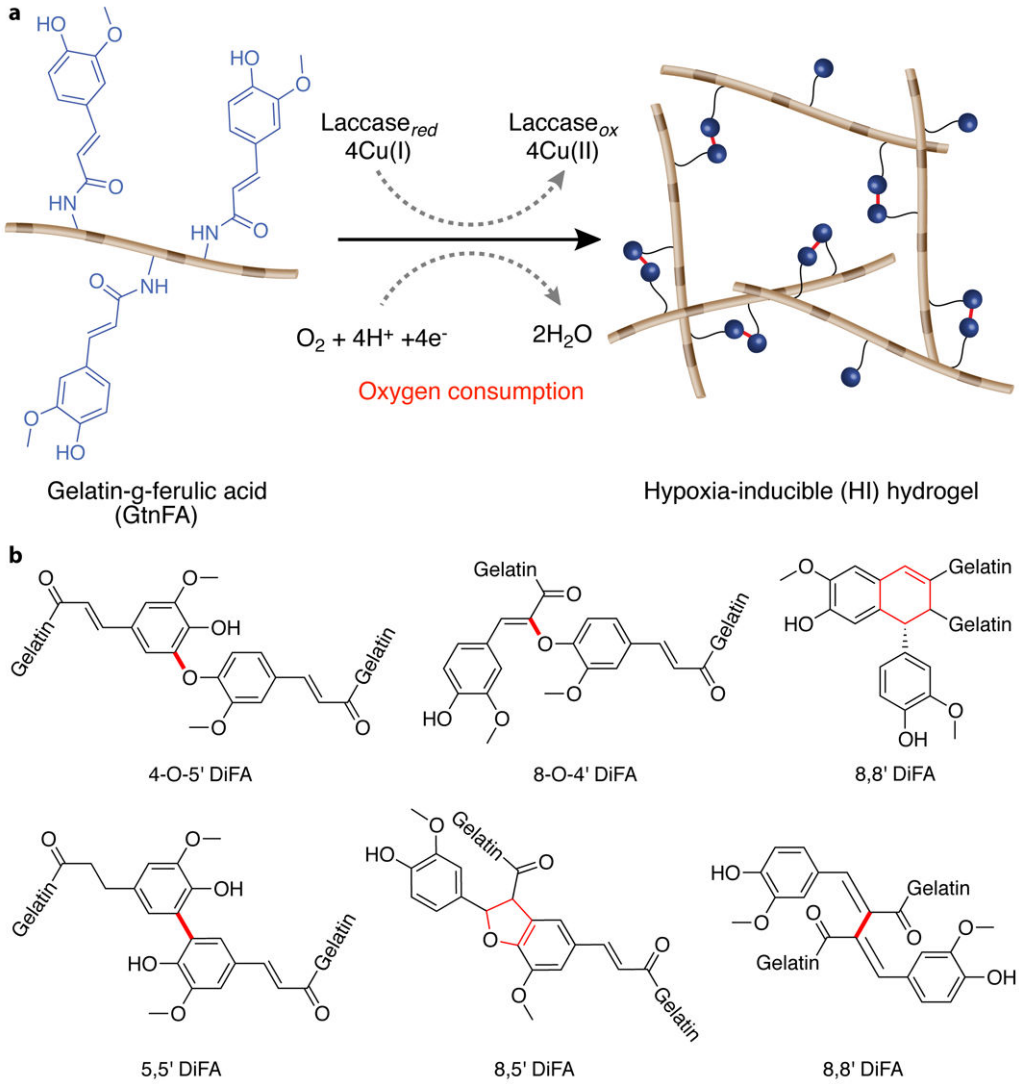

Figure 1. Hypoxia-inducible hydrogel synthesis and crosslinking chemistry

(**a**) Schematic representation of HI hydrogel formation. HI hydrogels are formed via laccase-mediated dimerization of FA molecules with oxygen consumption. Laccase catalyzes the four-electron reduction of molecular oxygen to water molecules, resulting in oxidation of FA molecules to form diferulic acid (DiFA), crosslinking the polymer networks. (**b**) Different chemical structures of DiFA could crosslink GtnFA polymer chains. Newly formed chemical structures are indicated in red.

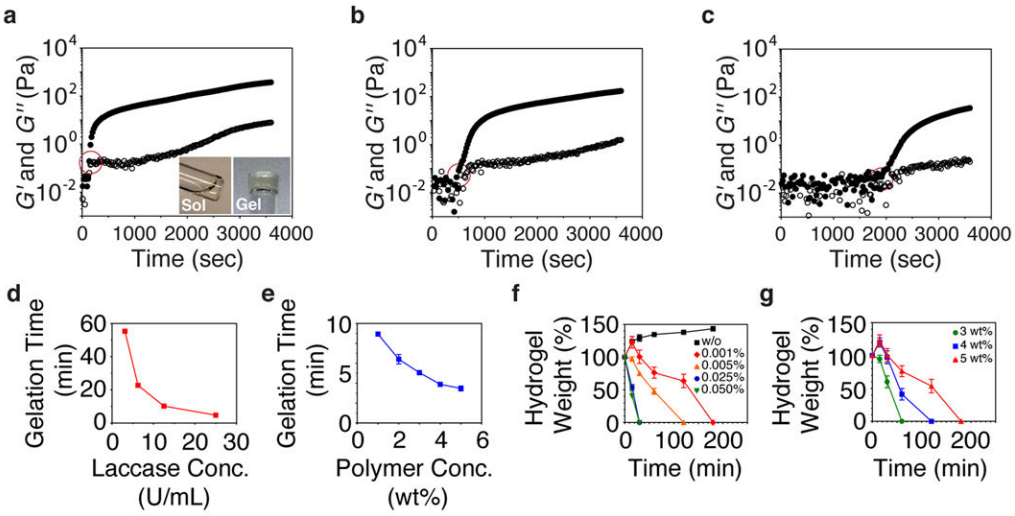

Figure 2. Network formation kinetics and proteolytic degradation of HI hydrogels

Elastic modulus (*G′*, filled symbols) and viscous modulus (*G″*, open symbols) of HI hydrogels as a function of time. Rheological analysis shows dynamic network formation and gelation kinetics for 3 wt% of HI hydrogel with laccase concentration of: (**a**) 25 U/ml (inset micrographs show sol-gel transition of the hydrogels); (**b**) 12.5 U/ml; and (**c**) 6.3 U/ml. Measurements were performed with constant strain of 10% and frequency of 0.1 Hz using 25 mm plate. Red circles represent the cross point of *G′* and *G″* indicating the gelation time. Effect of (**d**) laccase concentration and (**e**) polymer concentration on gelation time. Effect of (**f**) collagenase concentration and (**g**) polymer concentration on degradability. Results in d-g are shown as the average values ± SD ($n = 3$).

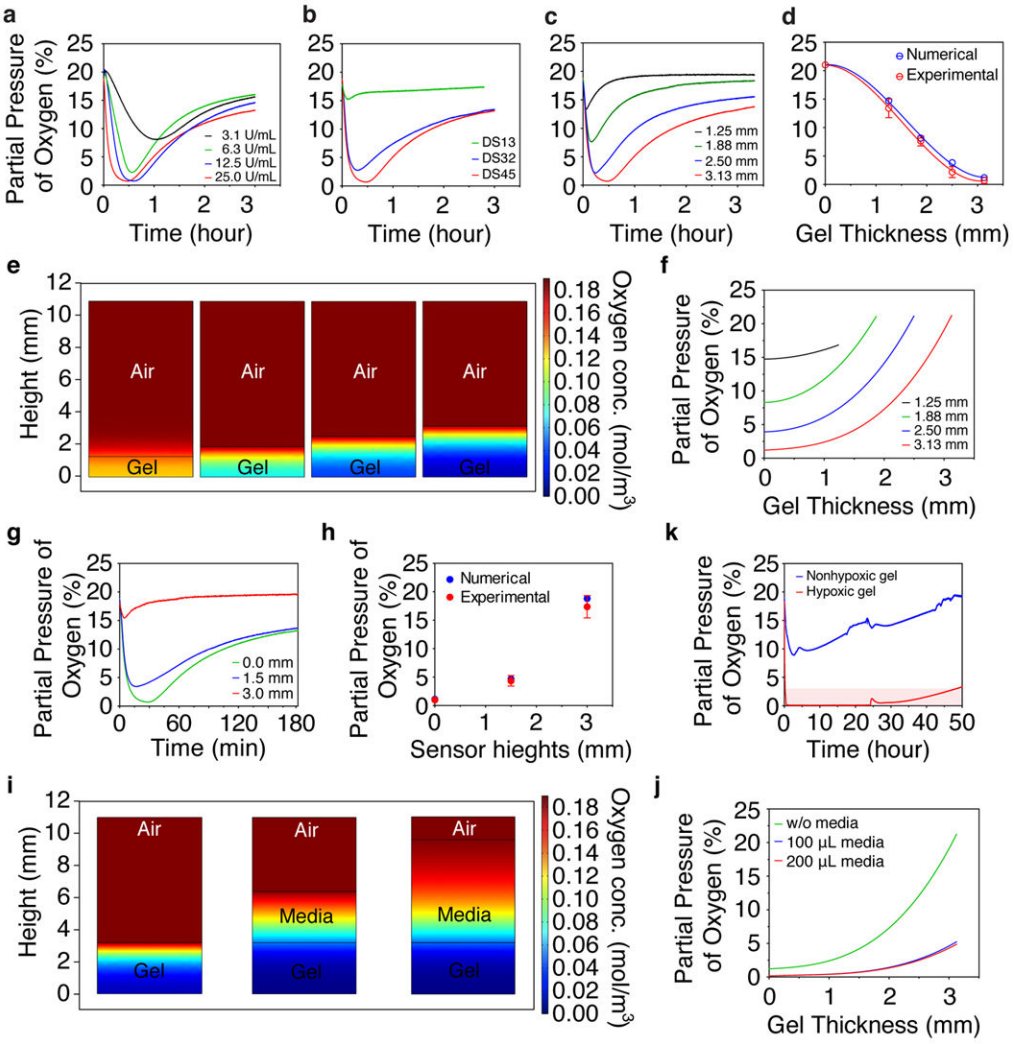

Figure 3. Controlling and predicting DO levels in HI hydrogel matrix

Measured DO levels in HI hydrogels as a function of time: (**a)** Effect of laccase concentration (3 wt%, DS 45, and 6.3–25.0 U/mL laccase). (**b)** Effect of degree of substitution (DS) of FA (3 wt%, 25 U/mL laccase, and 13–45 μmol/g of polymer). (**c)** Effect of hydrogel thickness (3 wt%, DS 45, and 25 U/mL laccase) (**d**) Model prediction of DO_{min} at the bottom of the HI hydrogels. We compared model numerical prediction (blue symbols) to the measured values (red symbols) to confirm the reliability of the given parameters; Model predictions of DO levels and gradients after 30 min of hydrogel formation (**e**) in the two-layer model (air-hydrogel) and (**f**) across HI hydrogels, depending on different thicknesses. Formation of DO gradients within HI hydrogels (3 wt%, DS 45, and 25 U/mL laccase) as indicated by (**g**) measured DO levels at different hydrogel depths as a function of time and (**h**) model prediction of DO_{min} at different hydrogel depths. We compared model numerical prediction (blue symbols) to the measured values (red symbols) to confirm the reliability of the given parameters. Model predictions of DO levels and gradients after 30 min of hydrogel formation (**i**) in the three-layer model (air-media-hydrogel) and (**j**) across the HI hydrogels with the culture media. (**k**) DO levels of HI hydrogels encapsulated with 2

× 10^6 cell/mL of ECFCs as a function of hydrogel thickness (hypoxic hydrogel thickness, 2.5 mm; nonhypoxic hydrogel thickness, 1.25 mm).

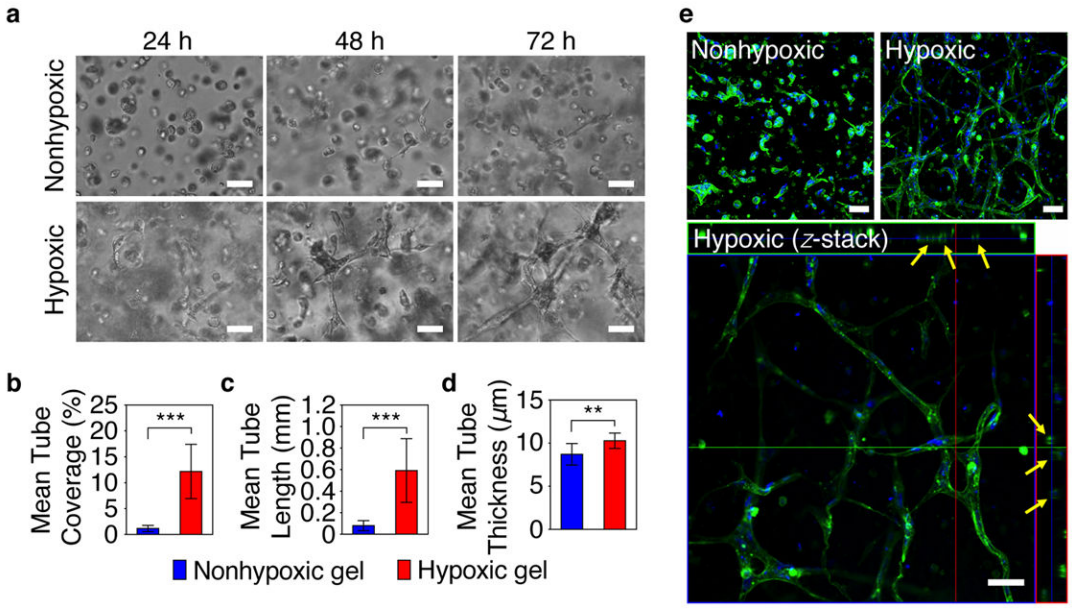

Figure 4. The HI hydrogel as a dynamic microenvironment for vascular morphogenesis

Vascular tube morphogenesis by ECFCs within the HI hydrogels. (**a**) Light micrographic images of ECFCs encapsulated within HI hydrogels during three days of culture. Scale bars are 50 μm. Quantitative analysis of vascular tube formation shows: (**b**) mean tube coverage, (**c**) tube length, and (**d**) tube thickness. Confocal microscopic images of ECFCs encapsulated within nonhypoxic gel and hypoxic gel; confocal *z*-stacks and orthogonal sections show lumen formation (indicated by arrows) within the vascular networks (phalloidin in green; nuclei in blue). Scale bars are 50 μm.

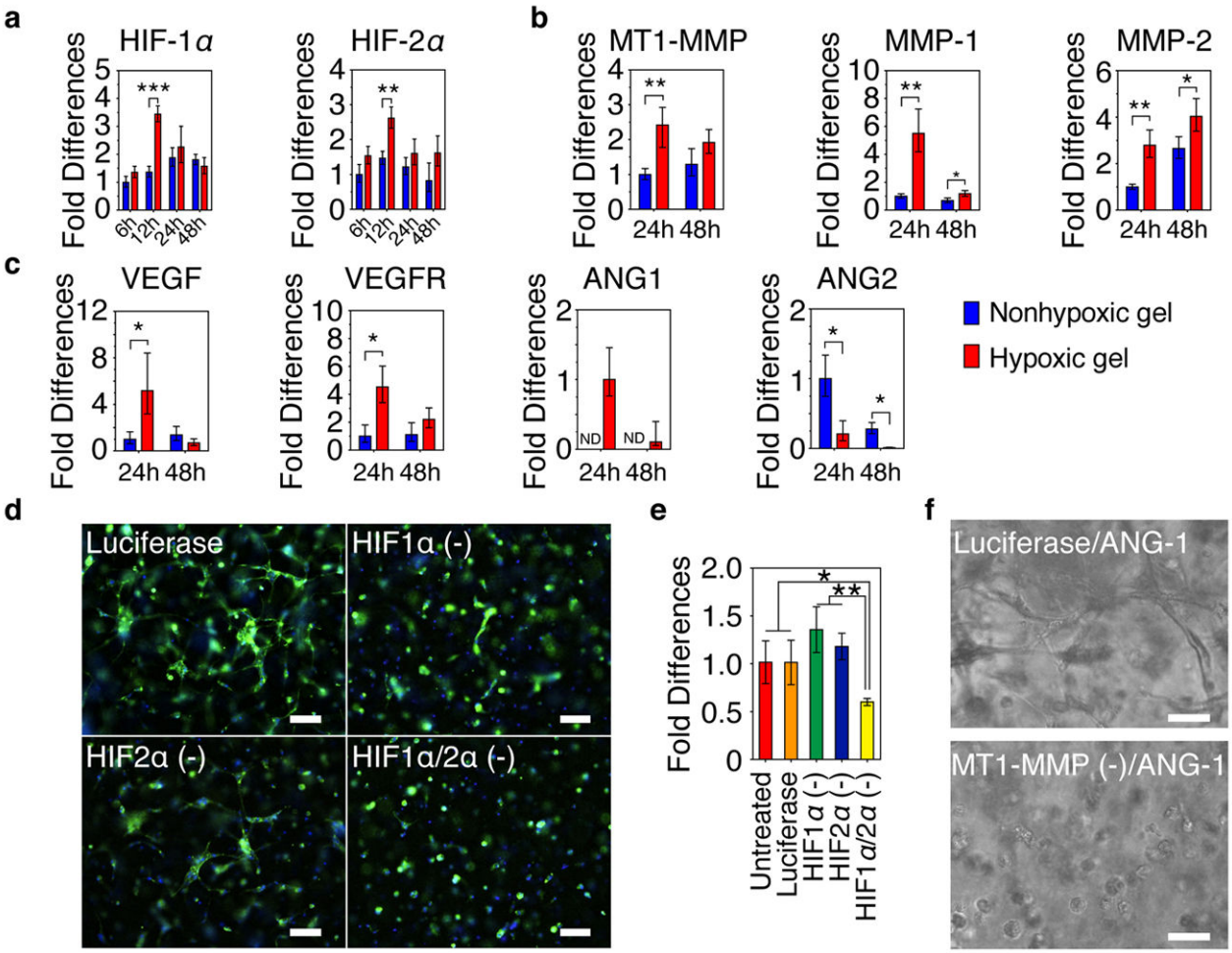

Figure 5. Molecular pathway activation of vascular morphogenesis within HI hydrogels

Real time RT-PCR analysis of gene expression of ECFCs encapsulated within the different hydrogel types: (**a**) HIFs, (**b**) *MMP* genes, and (**c**) *angiogenic* genes. (**d**) Inhibition of vascular morphogenesis of ECFCs by siRNA HIFs suppression. Fluorescence microscopic images after three days in culture show that siRNA suppression of HIF-1α and/or HIF-2α affect vascular morphogenesis. Scale bars are 50 μm. (**e**) Real time RT-PCR analysis of *MT1-MMP* gene expression of ECFCs treated with HIF-1α and/or HIF-2α siRNA and encapsulated within the HI gel after 24 h of culture. (**f**) Inhibition of vascular morphogenesis of ECFCs by siRNA MT1-MMP suppression. Light microscopy images after three days in culture show that siRNA suppression of MT1-MMPs affect vascular morphogenesis. Significance levels were set at: *$p < 0.05$, **$p < 0.01$, and ***$p < 0.001$. Values shown are mean ± SD. Scale bars are 25 μm.

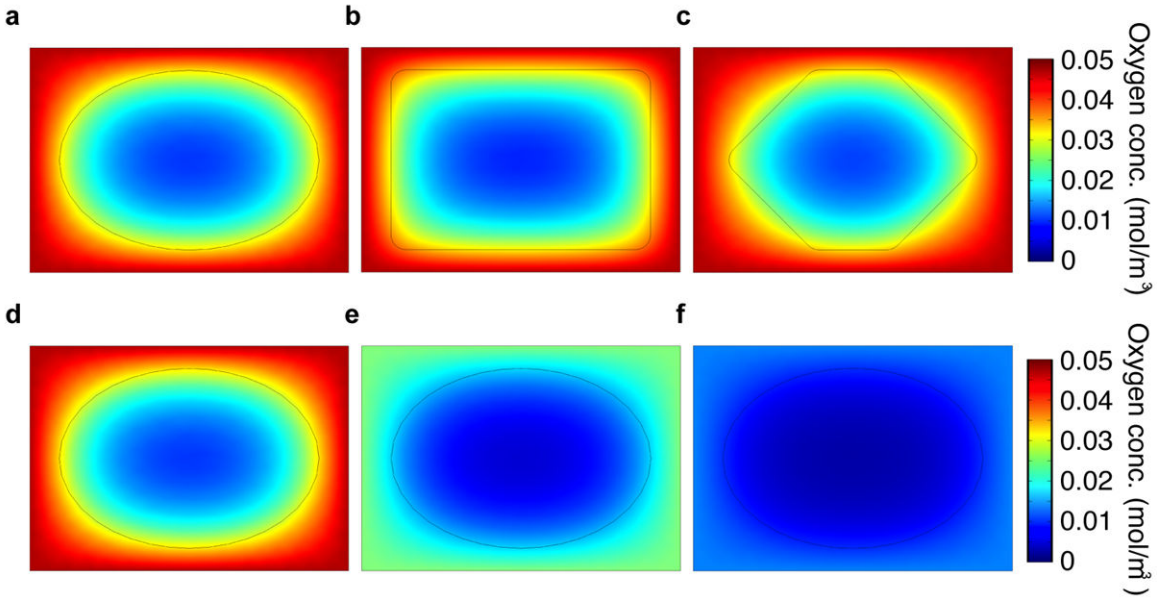

Figure 6. Model prediction of DO levels in dynamic *in vivo* environments

DO gradients within the HI hydrogels after 30 minute of injection depending on their shape; (**a**) eclipse, (**b**) rectangle, and (**c**) polygonal shapes. DO gradients within the HI hydrogels after 30 minutes of injection depending on different surrounding O_2 tensions, (**d**) 40 mmHg (DO levels of the hydrogel core, 8.4×10^{-3} mol/m^3; DO levels of the interface, 3.2×10^{-2} mol/m^3), (**e**) 20 mmHg (DO levels of the hydrogel core, 4.2×10^{-3} mol/m^3; DO levels of the interface, 1.7×10^{-2} mol/m^3) and (**f**) 10 mmHg (DO levels of the hydrogel core, 2.0×10^{-3} mol/m^3; DO levels of the interface, 0.8×10^{-2} mol/m^3).

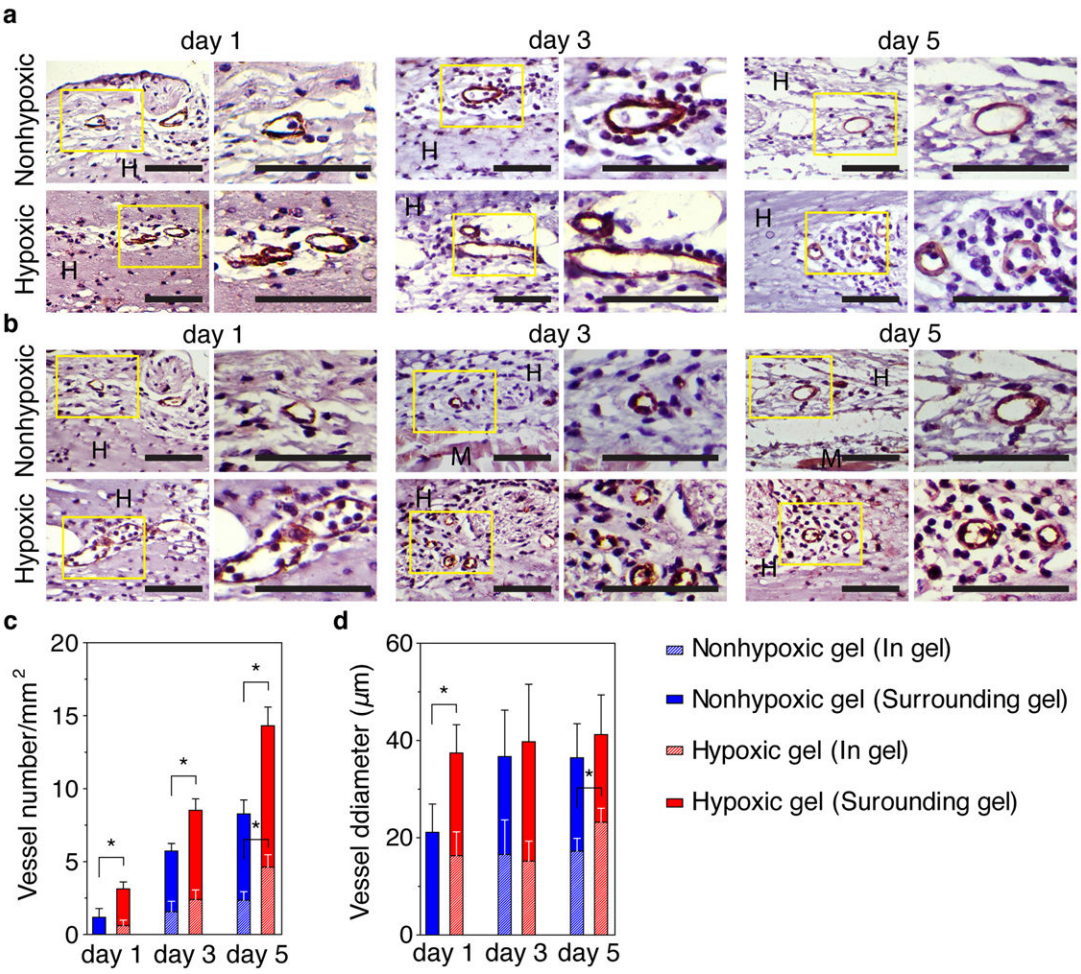

Figure 7. ***In vivo*** **angiogenic effect of the HI hydrogels**

Histological sections of hydrogels one, three and five days after injection stained with (**a**) α-SMA and (**b**) CD31.*Right panel* is high-magnification images of the boxed regions. Quantification of blood vessels number (**c**) and diameter (**d**) surrounding and penetrating into the hydrogels.M, Muscle; H, hydrogels. Significance levels were set at: $*p < 0.05$, $**p < 0.01$, and $***p < 0.001$.Scale bars are 100 μm.

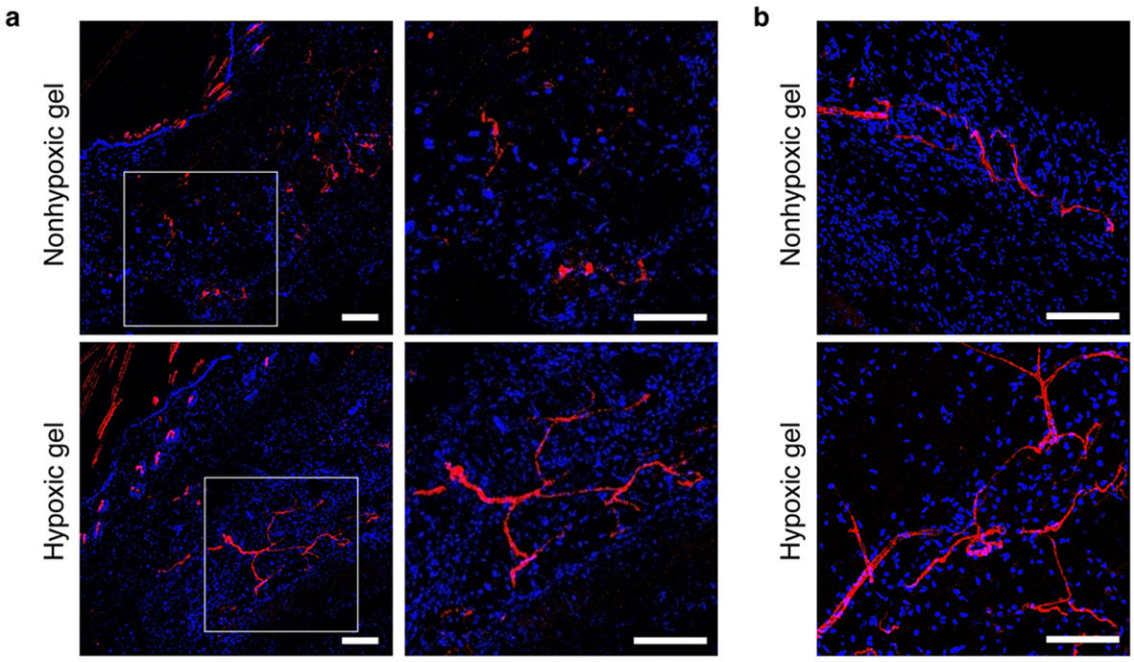

Figure 8. Blood vessel perfusion within the HI hydrogels a-b

Perfused blood vessels infiltrated into hydrogel matrix (**a**) three days and (**b**) five days after implantation. *GS-IB4* lectin in red and nucluei in blue. Values shown are mean ± SD. Scale bars are 100 μm.